Available online at www.elixirpublishers.com (Elixir International Journal)

Applied Mathematics

Elixir Appl. Math.109 (2017) 47908-47920

ISSN: 2229-712X

Double Diffusive Effects on MHD Free Convection Boundary Layer Casson Fluid Flow Past A Vertically Inclined Porous Plate: Thermal Radiation and Chemical Reaction Effects

P. Suresh[1], M. V.Ramana Murthy[2], S.Harising Naik[2] ,Chenna Krishna Reddy[2] and D.Bhagya[3]

[1]Department of Mathematics, Chaitanya Bharathi Institute of Technology, Gandipet, Hyderabad, Ranga Reddy District , 500075, Telangana State, India.

[2]Department of Mathematics& Computer Science, University College for Sciences, Osmania University, Hyderabad, 500007, Telangana State, India.

[3]Department of Mathematics , MVSR Engg College, Nadergul, Hyderabad, RR Dist, 501510, Telangana State, India.

ARTICLE INFO

Article history:

Received: 14 June 2017;

Received in revised form: 29 July 2017;

Accepted: 8 August 2017;

Keywords

MHD free convection, Casson fluid.

ABSTRACT

This work reports the numerical study of MHD free convection boundary layer flow of Casson fluid brought by vertically inclined porous surface in presence of thermal radiation and chemical reaction effects. Darcian viscous flow model for the porous medium is employed and the Rosseland diffusion approximation is used to describe the radiative heat flux in the energy equation. The homogeneous chemical reaction of first order is accounted in mass diffusion equation. The arising mathematically modelled non-linear partial differential equations of Casson fluid flow are successfully converted into linear coupled partial differential equations with the source of suitable transformation. The numerical solutions are computed through the application of finite difference method. The effect logs of an interesting physical parameters namely, Grashof number for heat and mass transfer, Magnetic field parameter, Permeability parameter, Prandtl number, Schmidt number, Thermal radiation parameter, Heat sink parameter, Chemical reaction parameter, Casson fluid parameter and Angle of inclination parameter number are discussed graphically. Further, the variations of skin-friction coefficient, heat and mass transfer rates are identified by way of tables. Comparison with the previous published literature is presented and an excellent agreement is reported.

Nomenclature

List of variables

B_0	Uniform magnetic field (*Tesla*)
x'	Coordinate axis along the plate (m)
y'	Co-ordinate axis normal to the plate (m)
u'	Velocity component in $x'-$ direction ($m\ s^{-1}$)
T'	Fluid Temperature (K)
T'_w	Fluid temperature at the wall (K)
T'_∞	Fluid temperature away from the plate (*K*)
C'	Fluid Concentration ($Kg\ m^{-3}$)
C'_w	Concentration of the plate ($Kg\ m^{-3}$)
y	Dimensionless displacement (m)
C'_∞	Concentration of the fluid far away from the plate ($Kg\ m^{-3}$)
C_p	Specific heat at constant pressure $\left(J\ Kg^{-1}K\right)$

Cf The local skin-friction $(N\ m^{-2})$

Nu The local Nusselt number Sh The local Sherwood number

u Fluid velocity ($m\ s^{-1}$)

D Solute mass diffusivity ($m^2\ s^{-1}$)

M Magnetic field parameter

Gr Grashof number for heat transfer

Gc Grashof number for mass transfer

$\Pr$ Prandtl number

Sc Schmidt number

R Thermal radiation parameter

Re Reynolds number

g Acceleration of gravity, 9.81 ($m\ s^{-2}$)

t Time (*sec*)

q_r Radiative heat flux

U_o Reference velocity ($m\ s^{-1}$)

Q Heat sink parameter

K Permeability parameter

Kr Chemical reaction parameter

k_e Mean absorption coefficient.

Greek Symbols

γ Casson fluid parameter

ν Kinematic viscosity ($m^2\ s^{-1}$)

ϕ Species concentration ($Kg\ m^{-3}$)

ρ The constant density ($Kg\ m^{-3}$)

β Volumetric coefficient of thermal expansion (K^{-1})

β^* Volumetric Coefficient of thermal expansion with concentration ($m^3\ Kg^{-1}$)

σ Electric conductivity of the fluid $(s\ m^{-1})$

θ Fluid temperature (K)

α Angle of inclination of plate ($\deg rees$)

τ'_w Shear stress $(N\ m^{-2})$

κ Thermal conductivity of the fluid (W/mK)

σ_s Stefan-Boltzmann Constant

Superscripts

$/$ Dimensionless Properties

Subscripts

w Conditions on the wall

∞ Free stream conditions

p Plate

1. Introduction

With the emerging importance of non-Newtonian fluids in recent industries and technology, mathematical modelling of non-Newtonian fluid flows and their understanding are of both fundamental and practical significance. The most important non-Newtonian fluid possessing a yield value is the Casson Fluid, which has significant applications in polymer processing industries and biomechanics. These Casson fluids have a yield stress below which no flow occurs and a zero viscosity at an infinite rate of shear. Some of the examples of Casson fluid are tomato sauce and soup, jelly and fruit juices, etc. The Casson constitutive equation was derived by Casson [1] and which shows that the rate of strain and stress relationship is nonlinear. Casson model constitutes a plastic fluid model which exhibits shear thinning characteristics, yield stress, and high shear viscosity.

According to a research conducted by Rao et al. [2], it is stated that Casson fluid model is reduced to a Newtonian fluid at a very high wall shear stress, i.e., when the wall stress is much greater than yield stress. This fluid model also approximates reasonably well the rheological behaviour of other liquids including physiological suspensions, foams, cosmetics, syrups, etc. Although different models are proposed to explain the behaviour of non-Newtonian fluids, the most important non-Newtonian fluid possessing a yield value is the Casson fluid. Bird et al. [3] investigated the rheology and flow of visco-plastic materials and reported that the Casson model constitutes a plastic fluid model which exhibits shear thinning characteristics, yield stress, and high shear viscosity. Fredrickson [4] investigated the steady flow of a Casson fluid in a tube. The unsteady boundary layer flow and heat transfer of a Casson fluid over a moving flat plate with a parallel free stream were studied by Mustafa et al. [5] and they solved the problem analytically using the Homotopy analysis method (HAM). Animasaun [6] presented the effects of some thermo-physical parameters on non-Darcian MHD dissipative Casson fluid flow along linearly stretching vertical surface when there exists migration of colloidal particles in response to a macroscopic temperature. Haq et al. [7] investigated the suction/injection effects on magnetohydrodynamic flow of a Casson nanofluid past a permeable exponentially shrinking surface and concluded that non-Newtonian fluid have higher friction factor compared with Newtonian fluid. Oyelakin et al. [8] studied unsteady convective Casson nanofluid flow over a stretching sheet in the presence of thermal radiation and slip boundary conditions. Hussanan et al. [9] studied an influence of Newtonian heating on Casson fluid past an oscillatory vertical plate by Laplace transform. Khalid et al. [10] found the exact solutions of an unsteady Magneto hydrodynamic natural convective flow of Casson fluid on an oscillatory vertical plate, with the absence of porous medium, magnetic field and viscous dissipation.

The fluid flow and heat transfer through a porous medium in presence of magnetic field have been extensively studied in the past because of its relevance to nuclear waste disposal, solid matrix heat exchanger, thermal insulation and other practical application. Natural convective flows are frequently encountered in physical and engineering problems such as chemical catalytic reactors, nuclear waste materials, and geothermal system. The concept of simultaneous heat and mass transfer is used in various science and engineering problems. It is used in food processing, wet-bulb thermometer and polymer solution and also in various fluids flow related engineering problems. In our daily life, the combined heat and mass transfer phenomenon is observed in the formation and dispersion of fog, distribution of temperature and moisture over agricultural fields and groves of fruit trees, crop damage due to freezing, and environmental pollution. Srinivasa Raju et al. [11] found both analytical and numerical solutions of unsteady MHD free convection flow over an exponentially moving vertical plate with heat absorption. Srinivasa Raju et al. [12] applied finite element method to unsteady MHD free convection flow past a vertically inclined porous plate including thermal diffusion and diffusion thermo effects. Combined influence of thermal diffusion and diffusion thermo on unsteady hydromagnetic free convective fluid flow past an infinite vertical porous plate in presence of chemical reaction studied by Srinivasa Raju [13]. Ramya et al. [14] studied boundary layer viscous flow of nanofluids and heat transfer over a nonlinearly isothermal stretching sheet in the presence of heat generation/absorption and slip boundary conditions. Srinivasa Raju et al. [15] studied unsteady MHD free convective flow past a vertical porous plate with variable suction. Chamkha and Khaled [16] investigated the problem of coupled heat and mass transfer by magnetohydrodynamic free convection from an inclined plate in the presence of internal heat generation or absorption. Sammer [17] investigated the heat and mass transfer over an accelerating surface with heat source in the presence of magnetic field. Naseem and Khan [18] investigated boundary layer flow past a stretching plate with suction, heat and mass transfer and with variable conductivity. Elbashbeshy and Bazid [19] studied flow and heat transfer in a porous medium over a stretching surface with internal heat generation and suction/blowing. Mohamed et al. [20] found analytical solutions of the unsteady MHD free convective heat and mass transfer flow past a semi-infinite porous regime adjacent to an infinite moving vertical plate with constant velocity. Cheng [21] reported the Soret and Dufour effects on natural convection heat and mass transfer from a vertical cone in a porous medium with uniform wall temperature and concentration (UWT/UWC). The Soret and Dufour effects on heat and mass transfer by natural convection from a vertical truncated cone in a fluid-saturated porous medium with variable wall temperature and concentration were studied by Cheng [22]. Makinde [23] studied the mixed convection flow with Soret and Dufour effects past a vertical plate embedded in a porous medium. Makinde et al. [24] used a numerical method to study of chemically-reacting hydromagnetic boundary layer flow with Soret/Dufour effects and a convective surface boundary condition.

Present study is the extension work of Mohamed et al. [20]. In this study we analyzed the flow, heat and mass transfer behaviour of Casson fluid past a vertically inclined plate in presence of thermal radiation, uniform magnetic field, heat sink and chemical reaction. The governing non-linear partial differential equations of the flow, heat and mass transfer are transformed into coupled linear differential equations by using similarity transformation and solved numerically using finite difference method. The effects of various non-dimensional governing parameters on velocity, temperature and concentration profiles are discussed and presented graphically. Also, the friction factor and Nusselt and Sherwood numbers are analyzed and given in tabular form for Casson fluid separately.

2. Mathematical formulation

In this investigation, unsteady MHD free convective heat and mass transfer Casson fluid flow of a viscous, incompressible, gray, absorbing-emitting but non-scattering, optically-thick and electrically conducting fluid occupying a vertically inclined porous regime with constant velocity is considered. The flow configuration of the problem is presented in Fig. 1. The following assumptions are restricted to this investigation.

i. The $x'-$ axis is taken along the vertical infinite porous plate in the upward direction and the $y'-$ axis normal to the plate.

ii. A constant magnetic field B_o is maintained in the y' direction and the plate moves uniformly along the positive x' direction with velocity U_0.

iii. At time $t' > 0$ a magnetic field of uniform strength is applied in the direction of y' – axis and the induced magnetic field is neglected.

iv. The temperature at the surface of the plate is raised to uniform temperature T_w' and species concentration at the surface of the plate is raised to uniform species concentration C_w' and is maintained thereafter.

v. Initially, for time $t' \le 0,$ the plate and the fluid are at some temperature T_∞' in a stationary condition with the same species concentration C_∞' at all points.

vi. The viscous dissipation and Ohmic dissipation of energy are negligible.

vii. The magnetic Reynolds number is so small that the induced magnetic field can be neglected.

viii. Also no applied or polarized voltages exist so the effect of polarization of fluid is negligible.

ix. All the fluid properties except the density in the buoyancy force term are constants.

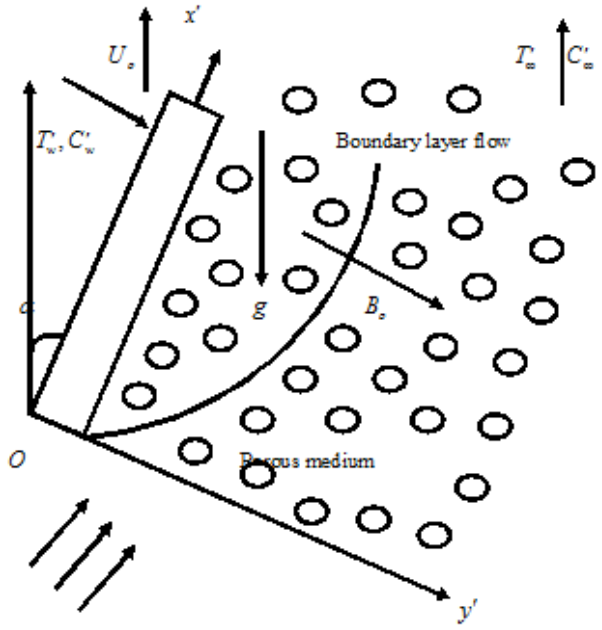

Fig 1. Schematic view of flow configuration.

The rheological equation of state for the Cauchy stress tensor of Casson fluid [25] is written as

$$\tau = \tau_0 + \mu\alpha^* \tag{1}$$

equivalently $$\tau_{ij} = \begin{cases} 2\left(\mu_B + \dfrac{p_y}{\sqrt{2\pi}}\right)e_{ij}, & \pi > \pi_c \\ 2\left(\mu_B + \dfrac{p_y}{\sqrt{2\pi_c}}\right)e_{ij}, & \pi < \pi_c \end{cases} \tag{2}$$

where τ is shear stress, τ_0 is Casson yield stress, μ is dynamic viscosity, α^* is shear rate, $\pi = e_{ij}e_{ij}$ and e_{ij} is the $(i, j)^{th}$ component of deformation rate, π is the product based on the non-Newtonian fluid, π_c is a critical value of this product, μ_B is plastic dynamic viscosity of the non-Newtonian fluid,

$$p_y = \frac{\mu_B\sqrt{2\pi}}{\gamma} \tag{3}$$

denote the yield stress of fluid. Some fluids require a gradually increasing shear stress to maintain a constant strain rate and are called Rheopectic, in the case of Casson fluid (Non-Newtonian) flow where

$$\mu = \mu_B + \frac{p_y}{\sqrt{2\pi}} \tag{4}$$

Substituting Eq. (3) into Eq. (4), then, the kinematic viscosity can be written as

$$\nu = \frac{\mu}{\rho} = \frac{\mu_B}{\rho}\left(1 + \frac{1}{\gamma}\right) \tag{5}$$

Under the above foregoing assumptions and Boussinesq's approximation, the equations governing the flow and transport reduce to the following equations:

Continuity Equation

$$\frac{\partial v'}{\partial y'} = 0 \tag{6}$$

Momentum Equation

$$\frac{\partial u'}{\partial t'} = \nu\left(1+\frac{1}{\gamma}\right)\frac{\partial^2 u'}{\partial y'^2} + g\beta(\cos\alpha)(T'-T'_\infty) + g\beta^*(\cos\alpha)(C'-C'_\infty) - \left(\frac{\sigma B_0^2}{\rho}\right)u' - \left(\frac{\nu}{K'}\right)u' \quad (7)$$

Energy Equation

$$\rho C_p \frac{\partial T'}{\partial t'} = \kappa \frac{\partial^2 T'}{\partial y'^2} - \frac{\partial q_r}{\partial y'} - Q_o(T'-T'_\infty) \quad (8)$$

Species Diffusion Equation

$$\frac{\partial C'}{\partial t'} = D\frac{\partial^2 C'}{\partial y'^2} - k'_r(C'-C'_\infty) \quad (9)$$

together with initial and boundary conditions

$$\left.\begin{array}{l} t' \le 0 : u' = 0,\ T' = T'_\infty,\ C' = C'_\infty \ \ for\ \ all\ \ y' \\ t' > 0 : \left\{\begin{array}{l} u' = U_o,\ T' = T'_w,\ C' = C'_w \ \ at\ \ y' = 0 \\ u' = 0,\ T' = T'_\infty,\ C' = C'_\infty \ \ as\ \ y' \to \infty \end{array}\right. \end{array}\right\} \quad (10)$$

For an optically thick fluid, in addition to emission there is also self absorption and usually the absorption co-efficient is wavelength dependent and large so we can adopt the Rosseland approximation for the radiative heat flux vector . Thermal radiation is assumed to be present in the form of a unidirectional flux in the direction i.e., (Transverse to the vertical surface). By using the Rosseland approximation [26] the radiative heat flux is given by

$$q_r = -\left(\frac{4\sigma_s}{3k_e}\right)\frac{\partial T'^4}{\partial y'} \quad (11)$$

It should be noted that by using the Rosseland approximation, the present analysis is limited to optically thick fluids. If temperature differences within the flow are sufficiently small, then equation (11) can be linearized by expanding in Taylor series about which after neglecting higher order terms takes the form

$$T'^4 \cong T'^4_\infty + 4(T'-T'_\infty)T'^3_\infty = 4T'T'^3_\infty - 3T'^4_\infty \quad (12)$$

Using Eq. (11) and (12) in the last term of Eq. (8), we obtain

$$\frac{\partial q_r}{\partial y'} = -\frac{16\sigma_s T'^3_\infty}{3k_e}\frac{\partial^2 T'}{\partial y'^2} \quad (13)$$

Introducing (13) in the Eq. (8), the energy equation becomes

$$\frac{\partial T'}{\partial t'} = \left(\frac{\kappa}{\rho C_p}\right)\frac{\partial^2 T'}{\partial y'^2} + \left(\frac{16\sigma_s T'^3_\infty}{3k_e\rho C_p}\right)\frac{\partial^2 T'}{\partial y'^2} - \frac{Q_o}{\rho C_p}(T'-T'_\infty) \quad (14)$$

We now introduce the following non-dimensional variables and parameters

$$\left.\begin{array}{l} u = \frac{u'}{U_o},\ y = \frac{y'U_o}{\nu},\ t = \frac{t'U_o^2}{\nu},\ \theta = \frac{T'-T'_\infty}{T'_w-T'_\infty},\ \phi = \frac{C'-C'_\infty}{C'_w-C'_\infty},\ M = \frac{\sigma B_o \nu}{\rho U_o^2},\ \mathrm{Re} = \frac{U_o x'}{\nu}, \\ Gr = \frac{g\beta\nu(T'_w-T'_\infty)}{U_o^3},\ Gc = \frac{\nu g\beta^*(C'_w-C'_\infty)}{U_o^3},\ \mathrm{Pr} = \frac{\nu\rho C_p}{\kappa},\ \ Sc = \frac{\nu}{D},\ Q = \frac{Q_o\nu}{\rho C_p U_o^2}, \\ K = \frac{\nu^2}{K'U_o},\ Kr = \frac{k'_r\nu}{U_o^2},\ R = \frac{16\sigma_s T'^3_\infty}{3k_e\kappa} \end{array}\right\} \quad (15)$$

The above defined non-dimensionless variables in Eq. (15) into Eqs. (7)-(9), and we get

$$\left(1+\frac{1}{\gamma}\right)\frac{\partial^2 u}{\partial y^2} - \frac{\partial u}{\partial t} - \left(M+\frac{1}{K}\right)u + Gr(\cos\alpha)\theta + Gc(\cos\alpha)\phi = 0 \quad (16)$$

$$(1+R)\frac{\partial^2\theta}{\partial y^2} - (\mathrm{Pr})\frac{\partial\theta}{\partial t} - (\mathrm{Pr})Q\theta = 0 \quad (17)$$

$$\frac{\partial^2\phi}{\partial y^2} - (Sc)\frac{\partial\phi}{\partial t} - (Sc)(Kr)\phi = 0 \quad (18)$$

with connected initial and boundary conditions

$$\left.\begin{array}{l} t \le 0 : u = 0,\ \theta = 0,\ \phi = 0 \ \ for\ \ all\ \ y \\ t > 0 : \left\{\begin{array}{l} u = 1,\ \theta = 1,\ \phi = 1 \ at\ \ y = 0 \\ u = 0,\ \theta = 0,\ \phi = 0 \ as\ \ y \to \infty \end{array}\right. \end{array}\right\} \quad (19)$$

For the design of chemical engineering systems and practical engineering applications, the local skin-friction, Nusselt number and Sherwood number important physical parameters for this type of boundary layer flow. The Skin-friction at the plate, which in the non-dimensional form is given by

$$Cf = \left(1+\frac{1}{\gamma}\right)\frac{\tau'_w}{\rho U_o \nu} = \left(1+\frac{1}{\gamma}\right)\left(\frac{\partial u}{\partial y}\right)_{y=0} \tag{20}$$

The rate of heat transfer coefficient, which in the non-dimensional form in terms of the Nusselt number is given by

$$Nu = -x'\frac{\left(\frac{\partial T'}{\partial y'}\right)_{y'=0}}{T'_w - T'_\infty} \Rightarrow Nu\,\mathrm{Re}^{-1} = -\left(\frac{\partial \theta}{\partial y}\right)_{y=0} \tag{21}$$

The rate of mass transfer coefficient, which in the non-dimensional form in terms of the Sherwood number, is given by

$$Sh = -x'\frac{\left(\frac{\partial C'}{\partial y'}\right)_{y'=0}}{C'_w - C'_\infty} \Rightarrow Sh\,\mathrm{Re}^{-1} = -\left(\frac{\partial \phi}{\partial y}\right)_{y=0} \tag{22}$$

3. Numerical Solutions by Finite Difference Method

The non-linear momentum and energy equations given in equations (16), (17) and (18) are solved under the appropriate initial and boundary conditions (19) by the implicit finite difference method. The transport equations (16), (17) and (18) at the grid point (*i*, *j*) are expressed in difference form using Taylor's expansion. The momentum equations reads.

$$\left(1+\frac{1}{\gamma}\right)\left(\frac{u_{i-1}^{j+1}-2u_i^{j+1}+u_{i+1}^{j+1}}{2(\Delta y)^2}+\frac{u_{i-1}^{j}-2u_i^{j}+u_{i+1}^{j}}{2(\Delta y)^2}\right)-\left(\frac{u_i^{j+1}-u_i^{j}}{\Delta t}\right)$$
$$+(Gr)(\cos\alpha)\left(\frac{\theta_i^{j+1}+\theta_i^{j}}{2}\right)+(Gc)(\cos\alpha)\left(\frac{\phi_i^{j+1}+\phi_i^{j}}{2}\right)-N\left(\frac{u_i^{j+1}+u_i^{j}}{2}\right)=0 \tag{23}$$

$$(1+R)\left(\frac{\theta_{i-1}^{j+1}-2\theta_i^{j+1}+\theta_{i+1}^{j+1}}{2(\Delta y)^2}+\frac{\theta_{i-1}^{j}-2\theta_i^{j}+\theta_{i+1}^{j}}{2(\Delta y)^2}\right)-(\mathrm{Pr})\left(\frac{\theta_i^{j+1}-\theta_i^{j}}{\Delta t}\right)-(\mathrm{Pr})Q\left(\frac{\theta_i^{j+1}+\theta_i^{j}}{2}\right)=0 \tag{24}$$

$$\left(\frac{\phi_{i-1}^{j+1}-2\phi_i^{j+1}+\phi_{i+1}^{j+1}}{2(\Delta y)^2}+\frac{\phi_{i-1}^{j}-2\phi_i^{j}+\phi_{i+1}^{j}}{2(\Delta y)^2}\right)-(Sc)\left(\frac{\phi_i^{j+1}-\phi_i^{j}}{\Delta t}\right)-(Kr)(Sc)\left(\frac{\phi_i^{j+1}+\phi_i^{j}}{2}\right)=0 \tag{25}$$

Where the indices and refer to and respectively. The initial and boundary conditions (19) yield

$$\left.\begin{aligned} &u_i^0 = 0,\ \theta_i^0 = 0,\ \phi_i^0 = 0 \quad for\ all\ i,\\ &u_i^j = 1,\ \theta_i^j = 1,\ \phi_i^j = 1\ at\ i = 0\ \&\ u_M^j \to 0,\ \theta_M^j \to 0,\ \phi_M^j \to 0 \end{aligned}\right\} \tag{26}$$

Thus the values of *u*, θ and ϕ at grid point *t* = 0 are known; hence the temperature and concentration profiles have been solved at time $t_{i+1} = t_i + \Delta t$ using the known values of the previous time $t = t_i$ for all $i = 1, 2, \ldots\ldots, N-1$. Then the velocity field is evaluated using the already known values of temperature and concentration profiles obtained at $t_{i+1} = t_i + \Delta t$. These processes are repeated till the required solution of *u*, θ and ϕ is gained at convergence criteria.

$$abs\left|(u,\ \theta,\ \phi)_{exact} - (u,\ \theta,\ \phi)_{numerical}\right| < 10^{-3} \tag{27}$$

4. Validation of Code

For code validation purpose, we compared our present numerical results with the exisistance analytical results of Mohamed et al. [20] in Fig. 2 in the absence of Casson fluid and Angle of inclination. From this figure, we observed that the relevant results obtained agree quantitatively with earlier results of Mohamed et al. [20].

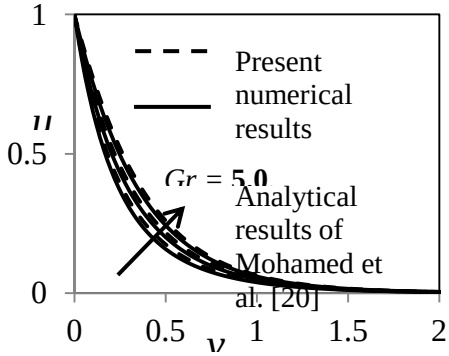

Fig 2. Comparison between present numerical results with the analytical results of Mohamed et al. [20] for different values of *Gr* in absence of Casson fluid and Angle of inclination.

5. Results and Discussions

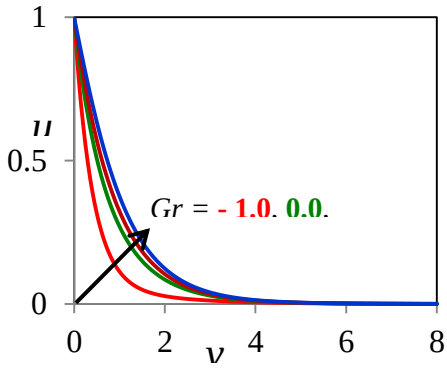

Fig 3. Gr influence on velocity profiles.

In order to point out the effects of various parameters such as Grashof number for heat transfer (Gr), Grashof number for mass transfer (Gc), Magnetic field parameter (M), Permeability parameter (K), Prandtl number (Pr), Schmidt number (Sc), Thermal radiation parameter (R), Heat absorption parameter (Q), Chemical reaction parameter (Kr), Casson fluid parameter (γ) and Angle of inclination parameter (α) are discussed in the following lines. on flow characteristic, the following discussion is set out. The values of Prandtl number are chosen Pr = 7 (water) and Pr = 0.71 (air). The value of the Schmidt number is chosen to represent the presence of species by hydrogen (0.22). The effect of these pertinent parameters is shown in the graphs. In the present study, the following default parameter values are adopted for computations: Gr = 2.0, Gc = 2.0, K = 0.5, M = 0.5, Q = 0.5, R = 0.5, Kr = 0.5, γ = 0.5 and α = 45o. All graphs therefore correspond to these values unless specifically indicated in the appropriate graph.

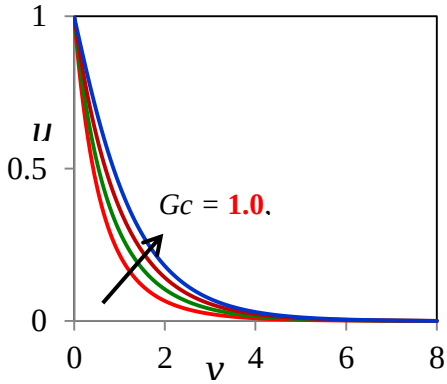

Fig 4. Gc influence on velocity profiles.

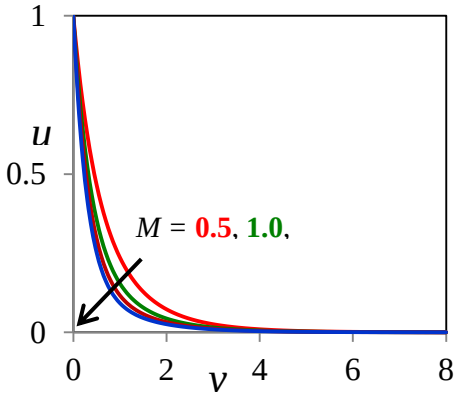

Fig 5. M influence on velocity profiles.

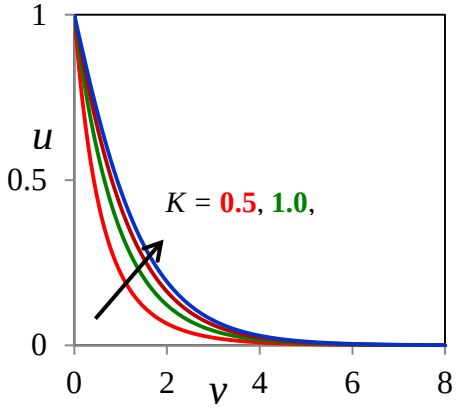

Fig 6. K influence on velocity profiles.

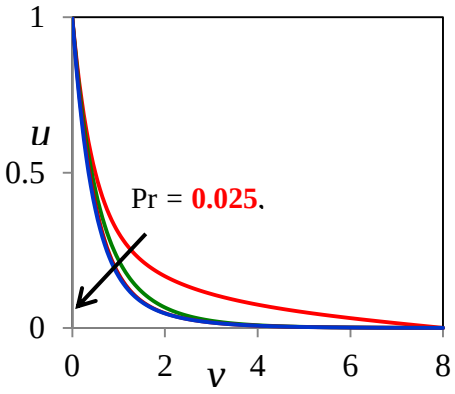

Fig 7. Pr influence on velocity profiles.

The velocity profiles for different values of Grashof number for heat transfer *Gr* are described in Fig. 3. It is observed that an increase in *Gr* leads to a rise in the values of velocity. Here the Grashof number for heat transfer represent the effect of free convection currents. Physically, $Gr > 0$ means heating of the fluid of cooling of the boundary surface, $Gr < 0$ means cooling of the fluid of heating of the boundary surface and $Gr = 0$ corresponds the absence of free convection current. The velocity profiles for different values ofGrashof number for mass transfer *Gc* are described in Fig. 4. It is observed that an increase in *Gc* leads to a rise in the values of velocity. Fig. 5 shows the effect of magnetic parameter *M* on the velocity. From this figure it is observed that velocity decreases, in both the cases of air and water, as the value of *M* is increased. This is due to the application of a magnetic field to an electrically conducting fluid produces a dragline force which causes reduction in the fluid velocity.

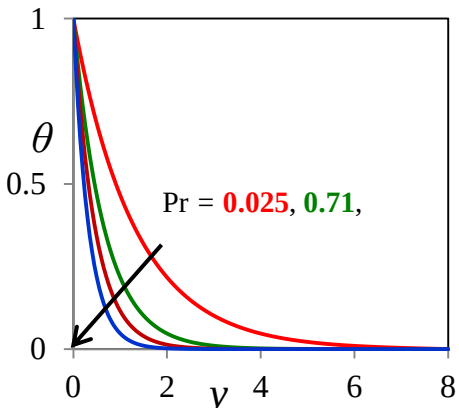

Fig 8. Pr influence on temperature profiles.

Fig. 6 depicts the velocity profiles for various values of *K*. From this figure it is observed that fluid velocity increases as *K* increases and reaches its maximum over a very short distance from the plate and then gradually reaches to zero for both water and air. Physically, an increase in the permeability of porous medium leads the rise in the flow of fluid through it. When the holes of the porous medium become large, the resistance of the medium may be neglected. Figs. 7 and 8 illustrate the velocity and temperature profiles for different values of Prandtl number. The numerical results show that the increasing values of Prandtl number, leads to velocity decreasing. From Fig. 8, the numerical results show that, the increasing values of Prandtl number leads to a decrease in the thermal boundary layer, and in general, lower average temperature within the boundary layer. The reason is that smaller values of Pr are equivalent to increasing the thermal conductivity of the fluid and therefore heat is able to diffuse away from the heated surface more rapidly for higher values of Pr. Hence, in the case of smaller Prandtl number, the thermal boundary layer is thicker and the rate of heat transfer is reduced.

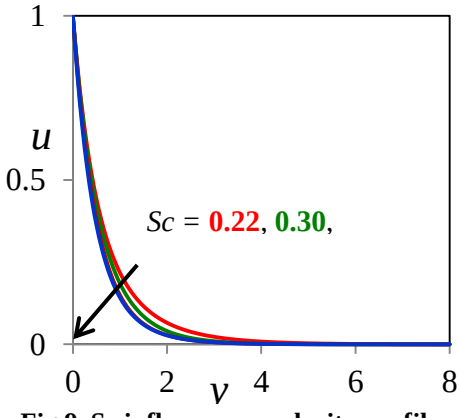

Fig 9. Sc influence on velocity profiles.

For various values of the Schmidt number *Sc*, the velocity and concentration are plotted in Figs. 9 and 10. As the Schmidt number increases, the concentration decreases. This causes the concentration buoyancy effects decrease, yielding a reduction in

the fluid velocity. Reductions in the velocity and concentration profiles are accompanied by simultaneous reductions in the velocity and concentration boundary layers.

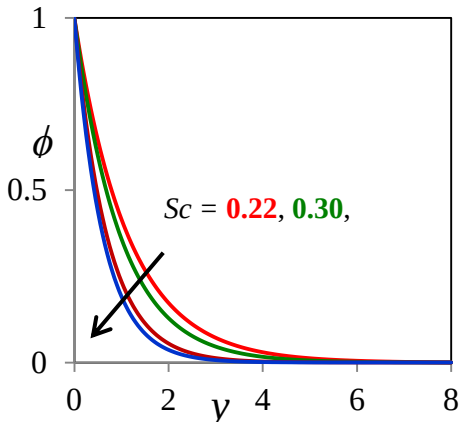

Fig 10. Sc influence on concentration profiles.

These behaviours are evident from Figs. 9 and 10. The effect of the thermal radiation parameter *R* on the velocity and temperature profiles in the boundary layer are illustrated in Figs. 11 and 12 respectively. Increasing the thermal radiation parameter *R* produces significant increase in the thermal condition of the fluid and its thermal boundary layer. This increase in the fluid temperature induces more flow in the boundary layer causing the velocity of the fluid there to increase. Figs. 13 and 14 has been plotted to depict the variation of velocity and temperature profiles against *y* for different values of heat source parameter *Q* by fixing other physical parameters. From this Graph we observe that velocity and temperature decrease with increase in the heat source parameter *Q* because when heat is absorbed, the buoyancy force decreases the temperature profiles.

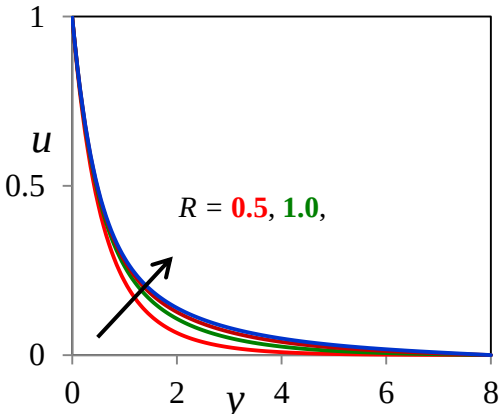

Fig 11. R influence on velocity profiles.

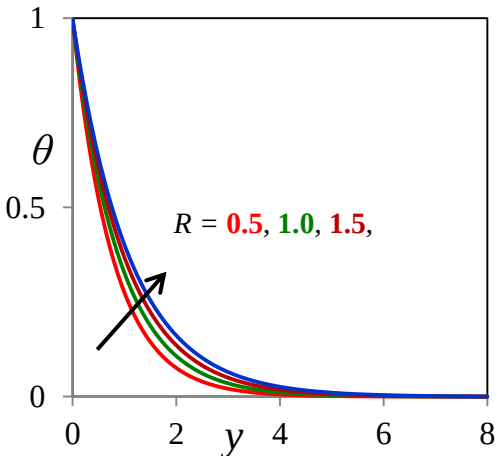

Fig 12. R influence on temperature profiles.

Fig. 15 displays the effect of the chemical reaction parameter Kr on the velocity profiles. As expected, the presence of the chemical reaction significantly affects the velocity profiles. It should be mentioned that the studied case is for a destructive chemical reaction Kr. In fact, as chemical reaction Kr increases, the considerable reduction in the velocity profiles is predicted, and the presence of the peak indicates that the maximum value of the velocity occurs in the body of the fluid close to the surface but not at the surface. Fig. 16 depicts the concentration profiles for different values of Kr, from which it is noticed that concentration decreases with an increase in chemical reaction parameter. This is due to the chemical reaction mass diffuses from higher concentration levels to lower concentration levels. The velocity profiles in the Fig. 17 shows that rate of motion is significantly reduced with increasing of Casson fluid parameter γ. Also, it is observed from this Fig. 17, the boundary layer momentum thickness decreases as increase of Casson fluid parameter γ. The effect of angle of inclination of the plate α on the

velocity field has been illustrated in Fig. 18. It is seen that as the angle of inclination of the plate α increases the velocity field decreases.

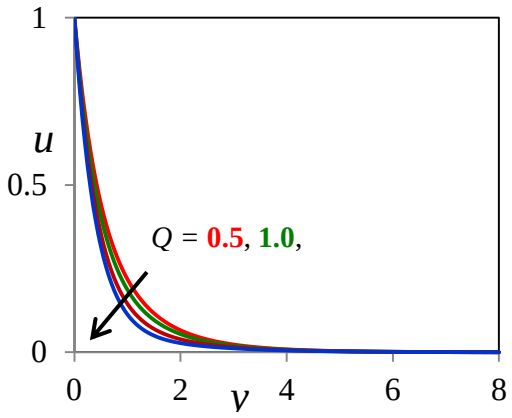

Fig 13. Q influence on velocity profiles.

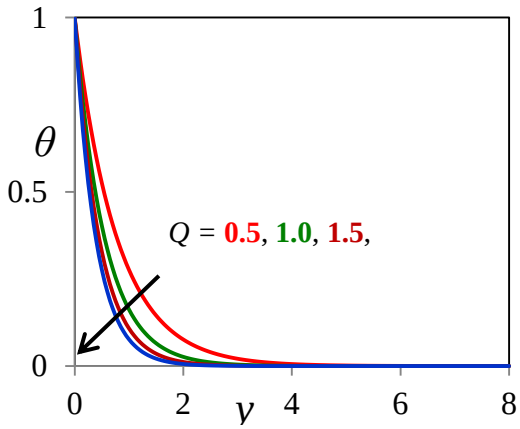

Fig 14. Q influence on temperature profiles.

The numerical computation of skin-friction coefficient is obtained and presented in table-1. It is observed that Magnetic field parameter, Prandtl number, Schmidt number, Chemical reaction parameter, Heat absorption parameter, Casson fluid parameter, Angle of inclination parameter decreases the skin-friction coefficient whereas it increases due to increase in Grashof number for heat transfer, Grashof number for mass transfer, Permeability parameter, Thermal radiation parameter.

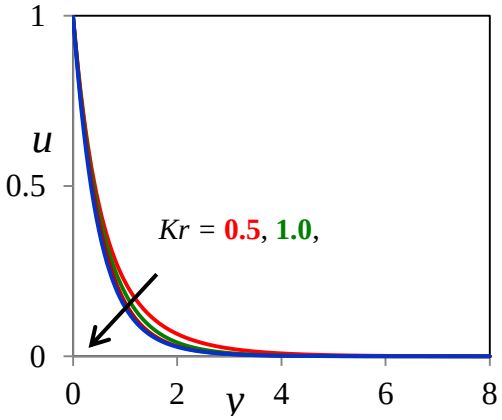

Fig 15. Kr influence on velocity profiles.

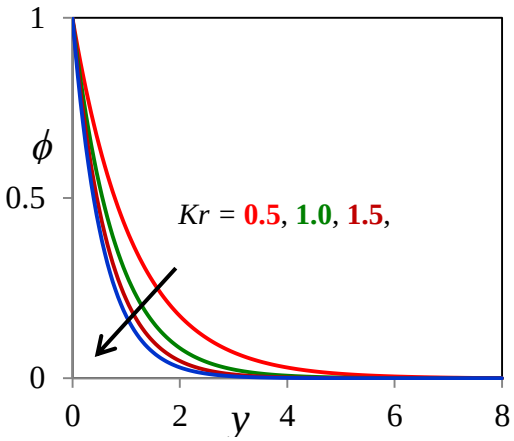

Fig 16. Kr influence on concentration profiles.

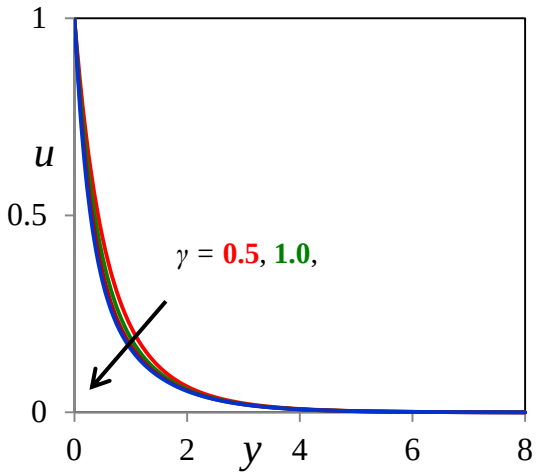

Fig 17. γ influence on velocity profiles.

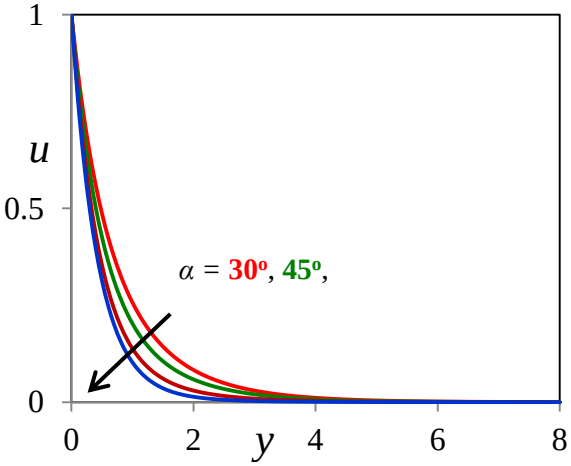

Fig 18. α influence on velocity profiles.

The numerical values of Nusselt and Sherwood numbers are presented in table-2. With increase in the Thermal radiation parameter, the Nusselt number increases but for the other parameters such as Prandtl number and Heat absorption parameter it decreases. A significant decrease is remarked in case of Sherwood number when there is an increase in the value of the Schmidt number and Chemical reaction parameter.

Table 1. Numerical values of Skin-friction coefficient.

Gr	*Gc*	*M*	*K*	Pr	*Sc*	*R*	*Q*	*Kr*	*γ*	*α*	*Cf*
2.0	2.0	0.5	0.5	0.71	0.22	0.5	0.5	0.5	0.5	45^o	- 1.2846875191
4.0	2.0	0.5	0.5	0.71	0.22	0.5	0.5	0.5	0.5	45^o	- 1.1655237675
2.0	4.0	0.5	0.5	0.71	0.22	0.5	0.5	0.5	0.5	45^o	- 1.0543143749
2.0	2.0	1.0	0.5	0.71	0.22	0.5	0.5	0.5	0.5	45^o	- 1.4110714197
2.0	2.0	0.5	1.0	0.71	0.22	0.5	0.5	0.5	0.5	45^o	- 1.2232890129
2.0	2.0	0.5	0.5	7.00	0.22	0.5	0.5	0.5	0.5	45^o	- 1.5358617306

2.0	2.0	0.5	0.5	0.71	0.30	0.5	0.5	0.5	0.5	45^o	- 1.3764232397
2.0	2.0	0.5	0.5	0.71	0.22	1.0	0.5	0.5	0.5	45^o	- 1.2459697723
2.0	2.0	0.5	0.5	0.71	0.22	0.5	1.0	0.5	0.5	45^o	- 1.3734459877
2.0	2.0	0.5	0.5	0.71	0.22	0.5	0.5	1.0	0.5	45^o	- 1.5072053671
2.0	2.0	0.5	0.5	0.71	0.22	0.5	0.5	0.5	1.0	45^o	- 1.3206881285
2.0	2.0	0.5	0.5	0.71	0.22	0.5	0.5	0.5	0.5	60^o	- 1.3004368544

Table 2. Numerical values of Nusselt and Sherwood numbers.

Pr	***R***	***Q***	***Nu***	***Sc***	***Kr***	***Sh***
0.71	0.5	0.5	1.5997371674	0.22	0.5	1.3697352409
7.00	0.5	0.5	1.1940317154	0.30	0.5	1.2269530296
0.71	1.0	0.5	1.3875653744	0.60	0.5	1.1187126637
0.71	0.5	1.0	1.6387772560	0.22	1.0	1.4032427692

6. Conclusions

In this paper, we have studied the effects of thermal radiation and heat absorption on unsteady MHD free convective Casson fluid flow and heat-mass transfer past an infinite vertically inclined plate with chemical reaction. Numerical analysis is made and the upshots are summarized as follows:

1. Velocity decreases with an increase in *M*, Pr, *Sc*, *Q*, *Kr*, γ and α while it increases with an increase in *Gr*, *Gc*, *K* and *R*.
2. Temperature increases with an increase in *R* while it decreases with an increase in Pr and *Q*.
3. Concentration decreases with an increase in *Sc* and *Kr*.
4. Local skin friction decreases for rising values of *M*, Pr, *Sc*, *Q*, *Kr*, γ and α while it increases with an increase in *Gr*, *Gc*, *K* and *R*.
5. Nusselt number increases with an increase in *R* while it decreases with an increase in Pr and *Q*.
6. Sherwood number decreases with an increase in *Sc* and *Kr*.
7. However, the results well agrees with the result of Mohamed et al. [20].

References

1. N. Casson, A flow equation for pigment oil-suspensions of the printing ink type, C.C. Mill (Ed.), Rheology of disperse systems, Pergamon Press (1959), p. 84.
2. A. S. Rao, V. R. Prasad, N. B. Reddy, O. A. Bég, Heat transfer in a Casson rheological fluid from a semi-infinite vertical plate with partial slip, Wiley Periodicals, Inc. (2013) http://dx.doi.org/10.1002/htj.21115.
3. R. B. Bird, G. C. Dai, B. J. Yarusso, The rheology and flow of viscoplastic materials, Rev Chem Eng, 1 (1983), pp. 1–83.
4. A. G. Fredrickson, Principles and applications of rheology, Prentice-Hall Englewood Cliffs, NJ, USA (1964).
5. M. Mustafa, T. Hayat, I. Pop, A. Aziz, Unsteady boundary layer flow of a Casson fluid due to an impulsively started moving flat plate, Heat Transfer, 40 (2011), pp. 563–576.
6. I. L. Animasaun, Effects of thermophoresis, variable viscosity and thermal conductivity on free convective heat and mass transfer of non-darcian MHD dissipative Casson fluid flow with suction and nth order of chemical reaction, J Nigerian Math Soc (2014) http://dx.doi.org/10.1016/j.jnnms.2014.10.008.
7. R. L. Haq, S. Nadeem, Z. H. Khan, T. G. Okedayo, Convective heat transfer and MHD effects on Casson nanofluid flow over a shrinking sheet, Cent. Eur. J. Phys, 12 (12) (2014), pp. 862–871.
8. Oyelakin, S. Mondal, P. Sibanda, Unsteady Casson nanofluid flow over a stretching sheet with thermal radiation, convective and slip boundary conditions, Alexandria Eng J, 55 (2) (2016), pp. 1025–1030.
9. A. Hussanan, M. Zuki Salleh, R. M. Tahar, I. Khan, Unsteady boundary layer flow and heat transfer of a casson fluid past an oscillating vertical plate with Newtonian heating, PLoS ONE, 9 (2014), p. 108763.
10. A. Khalid, Ilyas Khan, Sharidan Shafie, Exact solutions for unsteady free convection flow of casson fluid over an oscillating vertical plate with constant wall temperature, Abstr Appl Anal, 2015 (2015), Article 946350.
11. R. Srinivasa Raju, G. Jithender Reddy, J. Anand Rao, M. M. Rashidi, Rama Subba Reddy Gorla, Analytical and Numerical Study of Unsteady MHD Free Convection Flow over an Exponentially Moving Vertical Plate With Heat Absorption, International Journal of Thermal Sciences, Vol. 107, pp. 303 - 315, 2016.
12. R. Srinivasa Raju, B. Mahesh Reddy, M. M. Rashidi, Rama Subba Reddy Gorla, Application of Finite Element Method to Unsteady MHD Free Convection Flow Past a Vertically Inclined Porous Plate Including Thermal Diffusion And Diffusion Thermo Effects, Journal of Porous Media, Vol. 19, Issue. 8, pp. 701 - 722, 2016.
13. R. Srinivasa Raju, Combined influence of thermal diffusion and diffusion thermo on unsteady hydromagnetic free convective fluid flow past an infinite vertical porous plate in presence of chemical reaction, Journal of the Institution of Engineers: Series C, Vol. 97, Issue 4, pp. 505 - 515, 2016.
14. Ramya Dodda, R. Srinivasa Raju, J. Anand Rao, M. M. Rashidi, Boundary layer Viscous Flow of Nanofluids and Heat Transfer Over a Nonlinearly Isothermal Stretching Sheet in the Presence of Heat Generation/Absorption and Slip Boundary Conditions, International Journal of Nanoscience and Nanotechnology, Vol. 12, No. 4, pp. 251 - 268, 2016.
15. R. Srinivasa Raju, M. Anil Kumar, Y. Dharmendar Reddy, Unsteady MHD Free Convective Flow Past A Vertical Porous Plate With Variable Suction, ARPN Journal of Engineering and Applied Sciences, Vol. 11, No. 23, pp. 13608 - 13616, 2016.
16. A. J. Chamkha, A. R. A. Khaled, Similarity solutions for hydromagnetic simultaneous heat and mass transfer by natural convection from an inclined plate with internal heat generation or absorption, Heat Mass Transfer, 37 (2001), pp. 117–123.

17. A. A. Sammer, Heat and mass transfer over an accelerating surface with heat source in presence of magnetic field, IJTAM, 4 (2009), pp. 281–293.
18. A. Naseem, N. Khan, Boundary layer flow past a stretching plate with suction and heat transfer with variable conductivity, Int. J. Eng. Mater. Sci., 7 (2000), pp. 51–53.
19. E.M.A. Elbashbeshy, M.A.A. Bazid, Heat transfer in a porous medium over a stretching surface with internal heat generation and suction or injection, Appl. Math. Comput., 158 (2004), pp. 799–807.
20. R. A. Mohamed, Abdel-Nasser A. Osman, S. M. Abo-Dahab, Unsteady MHD double-diffusive convection boundary-layer flow past a radiate hot vertical surface in porous media in the presence of chemical reaction and heat sink, Meccanica (2013) 48:931–942, DOI 10.1007/s11012-012-9644-0.
21. C. Y. Cheng, Soret and Dufour effects on natural convection heat and mass transfer from a vertical cone in a porous medium, Int. Commun. Heat Mass Transfer, 36 (2009), pp. 1020–1024.
22. C. Y. Cheng, Soret and Dufour effects on heat and mass transfer by natural convection from a vertical truncated cone in a fluid-saturated porous medium with variable wall temperature and concentration, Int. Commun. Heat Mass Transf., 37 (2010), pp. 1031–1035.
23. O. D. Makinde, On MHD mixed convection with Soret and Dufour effects past a vertical plate embedded in a porous medium, Latin Am. Appl. Res., 41 (2011), pp. 63–68.
24. O.D. Makinde, K. Zimba, O. Anwar Bég, Numerical study of chemically-reacting hydromagnetic boundary layer flow with Soret/Dufour effects and a convective surface boundary condition, Int. J. Therm. Environ. Eng., 4 (2012), pp. 89–98.
25. Dash, R. K., Mehta, K. N., Jayaraman, G.: Casson Fluid Flow in a Pipe Filled with a Homogeneous Porous Medium. Int. J. Eng. Sci. 34, 1145-1156 (1996).
26. Brewster, M.Q., Thermal Radiative Transfer and Properties, John Wiley & Sons, New York, USA, (1992).